Research Article | Vol. 7, No. 7 | 1 Jul 2016 | BIOMEDICAL OPTICS EXPRESS 2849

Biomedical Optics EXPRESS

Imaging of targeted lipid microbubbles to detect cancer cells using third harmonic generation microscopy

KAITLIN HARPEL,[1,2,*] ROBERT DAWSON BAKER,[3] BABAK AMIRSOLAIMANI,[3] SOROUSH MEHRAVAR,[3] JOSEF VAGNER,[4] TERRY O. MATSUNAGA,[1,2] BHASKAR BANERJEE,[1,3,5] AND KHANH KIEU[3]

[1]*Department of Biomedical Engineering, University of Arizona, 1127 E. James E. Rogers Way, Tucson, Arizona, 85721, USA*
[2]*Department of Medical Imaging, College of Medicine, University of Arizona, 1609 N. Warren Ave., Tucson, Arizona, 85719, USA*
[3]*College of Optical Sciences, University of Arizona, 1603 E. University Blvd., Tucson, AZ, 85721, USA*
[4]*Ligand Discovery Laboratory, BIO5 Institute, University of Arizona, 1657 E. Helen Street, Tucson, AZ, 85721, USA*
[5]*Department of Medicine, College of Medicine, University of Arizona, 1501 N. Campbell, Tucson, Arizona, 85724, USA*
[*]*harpelka@email.arizona.edu*

Abstract: The use of receptor-targeted lipid microbubbles imaged by ultrasound is an innovative method of detecting and localizing disease. However, since ultrasound requires a medium between the transducer and the object being imaged, it is impractical to apply to an exposed surface in a surgical setting where sterile fields need be maintained and ultrasound gel may cause the bubbles to collapse. Multiphoton microscopy (MPM) is an emerging tool for accurate, label-free imaging of tissues and cells with high resolution and contrast. We have recently determined a novel application of MPM to be used for detecting targeted microbubble adherence to the upregulated plectin-receptor on pancreatic tumor cells. Specifically, the third-harmonic generation response can be used to detect bound microbubbles to various cell types presenting MPM as an alternative and useful imaging method. This is an interesting technique that can potentially be translated as a diagnostic tool for the early detection of cancer and inflammatory disorders.

OCIS codes: (020.4180) Multiphoton processes; (170.1610) Clinical applications; (190.1900) Diagnostic applications of nonlinear optics; (320.7090) Ultrafast lasers.

References and links

1. H. Chen, Z. Zhen, T. Todd, P. K. Chu, and J. Xie, "Nanoparticles for Improving Cancer Diagnosis," Mater. Sci. Eng. R. **74**, 35–69 (2013).
2. K. König, "Multiphoton microscopy in life sciences," J. Microsc. **200**(2), 83–104 (2000).
3. W. R. Zipfel, R. M. Williams, and W. W. Webb, "Nonlinear magic: Multiphoton microscopy in the biosciences," Nat. Biotechnol. **21**(11), 1369–1377 (2003).
4. F. Helmchen and W. Denk, "Deep tissue two-photon microscopy," Nat. Methods **2**(12), 932–940 (2005).
5. E. E. Hoover and J. A. Squier, "Advances in multiphoton microscopy technology," Nat. Photonics **7**(2), 93–101 (2013).
6. J. M. Denbeigh, B. A. Nixon, J. M. Hudson, M. C. Puri, and F. S. Foster, "VEGFR2-targeted molecular imaging in the mouse embryo: an alternative to the tumor model," Ultrasound Med. Biol. **40**(2), 389–399 (2014).
7. R. Kumar, W. S. Shin, K. Sunwoo, W. Y. Kim, S. Koo, S. Bhuniya, and J. S. Kim, "Small conjugate-based theranostic agents: an encouraging approach for cancer therapy," Chem. Soc. Rev. **44**(19), 6670–6683 (2015).
8. R. Williams, C. Wright, E. Cherin, N. Reznik, M. Lee, I. Gorelikov, F. S. Foster, N. Matsuura, and P. N. Burns, "Characterization of submicron phase-change perfluorocarbon droplets for extravascular ultrasound imaging of cancer," Ultrasound Med. Biol. **39**(3), 475–489 (2013).
9. G. Liu, K. Kieu, F. W. Wise, and Z. Chen, "Multiphoton Microscopy System with a Compact Fiber-based Femtosecond-pulse Laser and Handheld Probe," J. Biophotonics **4**(1-2), 34–39 (2011).
10. D. Yelin and Y. Silberberg, "Laser scanning third-harmonic-generation microscopy in biology," Opt. Express **5**(8), 169–175 (1999).

#262665 http://dx.doi.org/10.1364/BOE.7.002849
Journal © 2016 Received 11 Apr 2016; revised 17 Jun 2016; accepted 17 Jun 2016; published 28 Jun 2016

Biomedical Optics EXPRESS

11. G. O. Clay, A. C. Millard, C. B. Schaffer, J. Aus-der-Au, P. S. Tsai, J. A. Squier, and D. Kleinfeld, "Spectroscopy of third harmonic generation: Evidence for resonances in model compounds and ligated hemoglobin," J. Opt. Soc. Am. B **23**(5), 932–950 (2006).
12. M. J. Farrar, F. W. Wise, J. R. Fetcho, and C. B. Schaffer, "In vivo imaging of myelin in the vertebrate central nervous system using third harmonic generation microscopy," Biophys J. **100**, 1362–1371 (2011).
13. N. G. Horton, K. Wang, D. Kobat, C. G. Clark, F. W. Wise, C. B. Schaffer, and C. Xu, "In vivo three-photon microscopy of subcortical structures within an intact mouse brain," Nat. Photonics **7**(3), 205–209 (2013), doi:10.1038/nphoton.2012.336.
14. K. Kieu, S. Mehravar, R. Gowda, R. A. Norwood, and N. Peyghambarian, "Label-free multi-photon imaging using a compact femtosecond fiber laser mode-locked by carbon nanotube saturable absorber," Biomed. Opt. Express **4**(10), 2187–2195 (2013).
15. D. Bausch, S. Thomas, M. Mino-Kenudson, C. C. Fernández-del, T. W. Bauer, M. Williams, A. L. Warshaw, S. P. Thayer, and K. A. Kelly, "Plectin-1 as a novel biomarker for pancreatic cancer," Clin. Cancer Res. **17**(2), 302–309 (2011).
16. K. A. Kelly, N. Bardeesy, R. Anbazhagan, S. Gurumurthy, J. Berger, H. Alencar, R. A. Depinho, U. Mahmood, and R. Weissleder, "Targeted nanoparticles for imaging incipient pancreatic ductal adenocarcinoma," PLoS Med. **5**(4), e85 (2008).
17. S. Boitano, J. Hoffman, D. V. Tillu, M. N. Asiedu, Z. Zhang, C. L. Sherwood, Y. Wang, X. Dong, T. J. Price, and J. Vagner, "Development and evaluation of small peptidomimetic ligands to protease-activated receptor-2 (PAR2) through the use of lipid tethering," PLoS One **9**(6), e99140 (2014).
18. A. N. Flynn, J. Hoffman, D. V. Tillu, C. L. Sherwood, Z. Zhang, R. Patek, M. N. Asiedu, J. Vagner, T. J. Price, and S. Boitano, "Development of highly potent protease-activated receptor 2 agonists via synthetic lipid tethering," FASEB J. **27**(4), 1498–1510 (2013).
19. A. S. Huynh, W. J. Chung, H. I. Cho, V. E. Moberg, E. Celis, D. L. Morse, and J. Vagner, "Novel toll-like receptor 2 ligands for targeted pancreatic cancer imaging and immunotherapy," J. Med. Chem. **55**(22), 9751–9762 (2012).
20. P. S. Sheeran, T. O. Matsunaga, and P. A. Dayton, "Phase change events of volatile liquid perfluorocarbon contrast agents produce unique acoustic signatures," Phys. Med. Biol. **59**(2), 379–401 (2014).
21. J.-X. Cheng and X. S. Xie, "Green's function formulation for third-harmonic generation microscopy," J. Opt. Soc. Am. B **19**(7), 1604 (2002).
22. S. Francesco, Pavone and Paul J. Campagnola. *Second Harmonic Generation Imaging* (Boca Raton: CRC Taylor & Francis, 2014).
23. D. Débarre, W. Supatto, A. M. Pena, A. Fabre, T. Tordjmann, L. Combettes, M. C. Schanne-Klein, and E. Beaurepaire, "Imaging lipid bodies in cells and tissues using third-harmonic generation microscopy," Nat. Methods **3**(1), 47–53 (2006).
24. S. Witte, A. Negrean, J. C. Lodder, C. P. J. de Kock, G. Testa Silva, H. D. Mansvelder, and M. Louise Groot, "Label-free live brain imaging and targeted patching with third-harmonic generation microscopy," Proc. Natl. Acad. Sci. U.S.A. **108**(15), 5970–5975 (2011).
25. B. Weigelin, G.-J. Bakker, and P. Friedl, "Third harmonic generation of cells and tissue organization," J. Cell Sci. **129**, 245–255 (2016).
26. S. Mehravar, B. Banerjee, H. Chatrath, B. Amirsolaimani, K. Patel, C. Patel, R. A. Norwood, N. Peyghambarian, and K. Kieu, "Label-free multi-photon imaging of dysplasia in Barrett's esophagus," Biomed. Opt. Express **7**(1), 148–157 (2016).
27. C. G. Ethun and D. A. Kooby, "The importance of surgical margins in pancreatic cancer," J. Surg. Oncol. **113**, 283–288 (2015).
28. C. P. Raut, J. F. Tseng, C. C. Sun, H. Wang, R. A. Wolff, C. H. Crane, R. Hwang, J. N. Vauthey, E. K. Abdalla, J. E. Lee, P. W. Pisters, and D. B. Evans, "Impact of resection status on pattern of failure and survival after pancreaticoduodenectomy for pancreatic adenocarcinoma," Ann. Surg. **246**(1), 52–60 (2007).

1. Introduction

One fourth of all deaths in the United States are caused by cancer [1]. The diagnosis of cancer patients relies greatly on the time and accuracy of the detection of cancerous sites in the body. If the diagnosis can be made during the early stages of disease progression, then the prognosis for longer-term survival and even cure can be greatly increased [1]. The high probing sensitivity as well as large dynamic range of multiphoton microscopy makes it a potential imaging method for early detection of cancer and inflammatory markers in the body [2–5]. Inflammatory markers can be used to accurately localize and stage disease for appropriate therapy as well as assess effectiveness of that treatment (Theranostics). Therefore, there is a critical need for a novel diagnostic tool that cannot only detect disease, but also determine the surrounding tumor microenvironment through inflammatory markers to provide a more specialized therapy to the patient. Furthermore, with respect to surgical resections of cancerous tissue, a fast and reliable method for determining cancer-free margins

Biomedical Optics EXPRESS

intraoperatively that avoids the high sampling error associated with current methods of frozen-section microscopy of blind biopsies is of high priority.

In the past three decades, lipid microbubbles have been extensively explored as contrast agents to enhance ultrasound echoes in applications ranging from echocardiography to molecular imaging of vascularized tumors with a high degree of sensitivity. The diagnostic capability of lipid microbubbles (1-10 μm) for contrast-enhanced ultrasound (CEUS) is well established as an inexpensive and sensitive tool that provides both anatomical and functional information of tissue in real time [6]. A new technique, not yet approved in the clinical setting, is the use of targeted microbubbles as a diagnostic tool [7]. These ligand-conjugates decorated on the outer surface of microbubbles are designed for selectivity to an individual cell type over normal cells due to the overexpression of specific receptor proteins on the surface of these cells [7]. This development of targeted microbubbles could lead to additional diagnostic applications for CEUS as well as other imaging modalities such as; 1) early detection of cancerous lesions; 2) localization of inflammation; and 3) an especially large role in emerging theranostics [8]. The main application of this work aims to use targeted microbubbles with an alternative imaging modality, multiphoton microscopy, which can potentially be translated as a diagnostic tool for use in a surgical setting.

The motivation for this study is to develop a method whereby receptor-targeted lipid microbubbles can be used to ensure that all cancerous tissue has been removed during sugery for pancreatic cancer. Such a technique will allow the entire surgical margin to be analyzed for the presence of tumor cells during surgery, which is currently not possible. Although ultrasound easily images microbubbles intravenously, in an external environment **ultrasound requires a medium** between the transducer and the object being imaged. Pressure on the microbubbles from direct contact with ultrasound gel and a transducer can cause them to collapse or burst, leading to diagnostic inaccuracy. Moreover, this can become problematic when sterile environments need to be maintained. In order to increase simplicity and preserve accuracy, imaging modalities need to be explored that can detect microbubbles **directly** on a surface without the use of a contact medium. Multiphoton microscopy (MPM) has the ability to image **contact-free**, eliminating any concerns regarding contamination of a tissue surface. In addition, MPM can be miniaturized into a hand-held probe [9], making the imaging device easily applicable to, for example, intraoperative settings where point-of-care diagnostics can be utilized fast and efficiently.

The study described herein reports the successful imaging of microbubbles using a multi-photon microscope with compact femtosecond fiber lasers operating at 1560 nm and 1040 nm. In particular, we were able to explore via contact-free imaging, the binding of receptor-targeted lipid microbubbles *in vitro* on pancreatic tumor cell culture, using third-harmonic generation (THG). Compared to fluorescence detection, THG does not require an external marker and has a much larger dynamic range and thus a larger probing sensitivity [10–14]. This has the potential to provide the accuracy and specificity required for detection of cancer in earlier stages, as well as inflammatory markers in the body. To show the capability of our technique, we investigate the detection of plectin-targeted lipid microbubbles, as these receptors are overexpressed in pancreatic cancer cell lines [15]. To our knowledge, the detection of targeted microbubbles using THG is a novel application for MPM and could pertain to a wide range of diagnostic applications.

2. Sample preparation and experimental setup

2.1 Sample preparation of targeted lipid microbubbles

Plectin-1 was recently identified as a receptor biomarker to detect pancreatic ductal adenocarcinoma (PDAC). This receptor is identified in 100% of tested PDAC tumors and 60% of pre-invasive PanIN III lesions [15]. Immunohistochemistry of human tissue has shown that Plectin-1 is not expressed by most normal tissue, with the exception of the skin and genitourinary tract. Plectin-1 specific ligand was panned from a phage display screen

Biomedical Optics EXPRESS

reported previously [16]. We have adopted a peptide ligand for specific targeting of PDAC in our lipid microbubble imaging. A peptide was attached to the bis-palmitoyl lipid-like moiety via a short polyethyleneglycol spacer (extended span distance ~140Å). The specific peptide sequence was Lys-Thr-Leu-Leu-Pro-Thr-Pro-NH_2. The synthesis of lipidated ligand was performed by solid-phase technology using a Fmoc/tBu protection strategy [17–19].

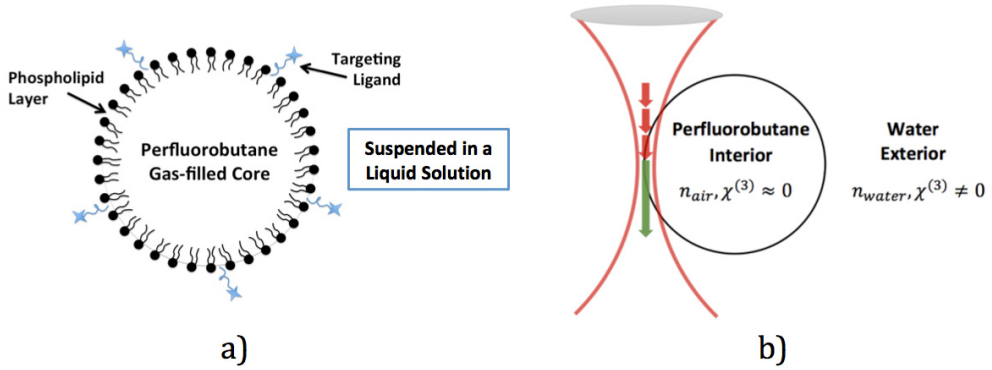

Fig. 1. **a)** The basic components of the lipid microbubble used in the experiment. The specific targeted ligand (KTLLPTP) used was selective for the plectin-1 receptor. **b)** Microbubble and focused femtosecond laser beam interaction. THG signal is expected to be generated strongly from the liquid/gas interface.

The lipid microbubble formulation is depicted in Fig. 1. The bubbles were prepared with a lipid composition containing dipalmitoylphosphatidylcholine (DPPC) (Genzyme, Cambridge, MA, USA), 1,2-dipalmitoyl-*sn*-glycero-3-phosphate (monosodium salt) (DPPA) (Avanti Polar Lipids, Alabaster, AL, USA), and our lipidated ligand targeting pancreatic cancer cells. The lipid composition was dispersed in an excipient solution of phosphate-buffered saline (PBS), propylene glycol, and glycerol for a total lipid concentration of 1 mg mL^{-1}. From this lipid solution, 1.5 mL was pipetted into a 2 mL glass vial (Wheaton Industries, Millville, NJ), and the air headspace was then replaced with decafluorobutane (DFB) gas (Fluoromed, Round Rock, TX, USA). The microbubbles were then formed by mechanical agitation using a modified dental amalgamator (Lantheus Medical, New York, NY), resulting in a microbubble distribution ranging predominantly from 1 −10 μm with a concentration of 1-5 x 10^9 microbubbles per mL of solution [20]. The liquid microbubble is imaged using a tightly focused femtosecond laser beam, which is scanned across it. THG signal is expected to be generated strongly from the liquid/gas interface.

2.2. Cell culture

The pancreatic cancer cell lines PANC-1 and MIA-PaCa2, which have amplified plectin expression, were grown in the University of Arizona Cancer Center using Dulbecco's Modified Eagle's Medium (DMEM) with 4.5 g/L glucose, L glutamine, and sodium pyruvate, supplemented with 10% fetal bovine serum and 1% penicillin-streptomycin. The cells were incubated in a 5% carbon dioxide, humidified atmosphere at 37° C. Cells were detached with trypsin and transferred onto poly-d-lysine coated glass bottom dishes (Mat Tek, Ashland, MA) followed by incubation for an additional 24 hours to ensure adherence.

2.3. Multiphoton microscope

Multi-photon (MP) imaging is a powerful technique that allows three dimensional mapping of samples that have a measurable nonlinear optical response such as second harmonic generation, third harmonic generation, or fluorescence induced by MP absorption. MP imaging (MPI) is currently an important tool for biological research and efforts are underway

Biomedical Optics EXPRESS

to turn this useful imaging technology into robust instruments for clinical applications [2–5]. Lipid microbubbles are small, spherical structures formed by a thin lipid layer and contain a biocompatible gas (e.g. DFB) inside. These bubbles are typically dispersed in a liquid medium where they can attach to binding sites if their lipid membrane is functionalized with a suitable ligand.

There exists a transition from liquid phase to gas phase at the surface of the bubbles, stabilized by a thin lipid membrane. For that reason, ultrasound has been used to detect these bubbles due to the large scattering of ultrasound signal at their liquid/gas interfaces. In optics, third harmonic generation (THG) is a nonlinear optical effect, which arises from the third order nonlinear optical response of a material. THG has been shown to be very useful in label-free multiphoton imaging [10–14]. Due to the Gouy phase shift in a tightly focused laser beam, the THG signal is generated only from interfaces where there is a change in the refractive index (or change in the third order nonlinear response). Hence, THG has been shown to be useful in detecting these interfaces in biological tissues, such as lipid bodies in cells [21–23]. Given the above, we hypothesized that THG should be useful as a contactless detection of targeted lipid microbubbles given the sudden liquid/gas transition that these bubbles exhibit.

The design and performance of our home-built microscope has been published previously [14]. The new feature that we added to the system is a new femtosecond laser operating at 1040 nm which emits ~70 mW average power at ~8 MHz repetition rate and ~100 fs pulse duration. The microscope can accommodate both 1560 nm and 1040 nm without changing the optics in the excitation beam path. The addition of the 1040 nm laser allows us to excite the marker dye, DiI, which we use to colocalize the fluorescence marker with the THG signal (described below) to confirm that we indeed detect THG from the liquid/gas interface of the bubbles. The dichroic filter and bandpass filter in front of the photomultiplier tube (PMT) for THG signal detection are changed to match the new excitation wavelength respectively. Specifically, we use a 345 nm bandpass filter (~20 nm pass band) in front of the PMT to detect the THG signal. A pump filter (Semrock, FF01-750/SP-25) is also used to remove pump laser light from reaching the PMTs. A 520 nm bandpass filter is used with the 1560 nm excitation laser to pass only the THG signal. The diagram of the microscope can be seen in Fig. 2.

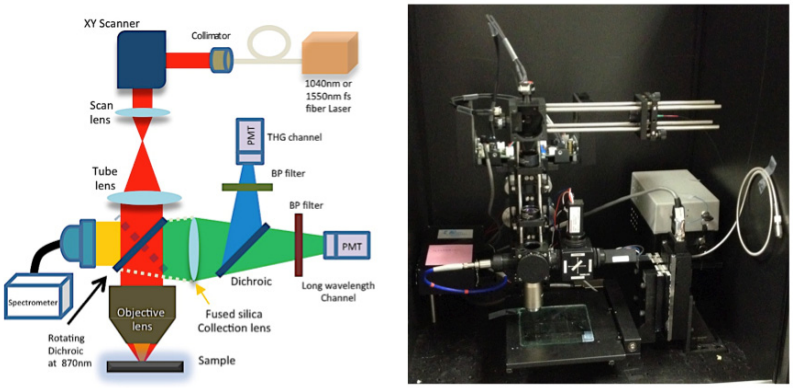

Fig. 2. Left: Schematic diagram of our home-built multiphoton microscope. The system has a THG spot size of ~350 nm and an axial resolution of 2µm (with a Nikon 40x objective, NA 1.3) at the excitation wavelength of 1040nm. The system has a THG spot size of ~525 nm and an axial resolution of 3 µm (with a Nikon 40x objective, NA 1.3) at the excitation wavelength of 1560nm. Right: A photograph of the microscope where both excitation laser sources are visible. The 1560nm laser is the the gray box on top and the 1040nm laser source is the black box at the bottom. A Ocean Optics spectrometer (350nm-1100nm detection range) is integrated into the multiphoton microscope for measuring the optical spectrum of the multiphoton excited signals (black box with blue input fiber on the left).

Biomedical Optics EXPRESS

3. Experimental set up and results

3.1 Theoretical description of THG generated MPM signal

Experimental imaging results for these microbubbles indicate that MPM signals are dominated by THG at the interface resulting from a difference in bulk third-order susceptibilities. However, imaging results also display an unexpected signal in the center of the microbubbles, which is a gaseous area with no interface change. Our research group is pursuing the reason for this unexpected signal. To model this, we approximate the DFB interior as air ($n_{interior}(\lambda) \approx n_{air}(\lambda), \chi^{(3)} \approx 0$ –linear, dispersive and isotropic) and the exterior as water ($n_{exterior}(\lambda) \approx n_{water}(\lambda), \chi^{(3)} \approx \chi^{(3)}_{water}$ –nonlinear, dispersive, and isotropic). Because the boundary lipid monolayer is very small in scale (< 10 nm) and because live cell walls (water inside and outside) have not generated an appreciable MPM signal in our experimental configuration, we neglect any nonlinear polarizability of the lipid layer itself. The fact that we are predominantly resolving interfaces in this experiment is explained by the Gouy phase shift, which in bulk media (no interfaces) causes destructive interference of the THG when integrated over the entire focal volume [21]. When the pump field encounters spatial variation of $\chi^{(3)}$, the coupling from third harmonic to the pump field is distorted spatially and this destructive interference cannot occur. Thus, the signal that we obtain in this experiment is dominated by spatial variation of $\chi^{(3)}$. The strength of the generated signal in the moderate focusing case (NA < 1) has been reported as [22]:

$$I_{3\omega} \propto \kappa \left| \frac{\chi^{(3)}_{water}}{n_{3\omega}(n_{3\omega} - n_{\omega})} \right|^2 I_{\omega}^3$$

And in the strong focusing case (NA > 1) as [22]:

$$I_{3\omega} \propto \kappa \left| \chi^{(3)}_{water} \right|^2 I_{\omega}^3$$

This model is relevant for the central wavelength of a pulse in a carrier-envelope model. Large spectral bandwidths are expected to lead to longitudinal chromatic aberration and consequently to low resolution of the microscope in the *z* direction. This causes THG images to deviate from the expected donut shape at the center *z*-plane for smaller bubbles.

Detailed theoretical modeling is being pursued in our research group to get a deeper understanding of the THG generation process from these lipid microbubbles. The theoretical modeling and simulation results turn out to be quite complex and thus are beyond the scope of this paper.

3.2 Imaging of lipid microbubbles to verify the signal obtained from MPM is THG

The water-air interface in the lipid microbubble generates a THG signal that is demonstrated in Fig. 3. The image on the right, Fig. 3(b), shows the THG signal generated from the lipid microbubbles through the use of a filter that separates the THG signal into the corresponding PMT detector. The image on the left, Fig. 3(a), shows lipid microbubbles bound to a surface imaged with confocal microscopy (for comparison purpose). The microbubbles could not be imaged with confocal microscopy in a solution, as in Fig. 3(b), because the mixture contains residual DiI molecules that do not insert into the membrane of the bubbles. Since confocal microscopy only detects fluorescent signal, the imaging resolution is not high enough to separate the signal from the DiI molecules on the microbubble membrane from the residual DiI in the surrounding solution. Therefore to obtain Fig. 3(b), we had to allow the lipid microbubbles to bind to the bottom of a petrie dish and then wash the remaining bubble solution off the dish so that only the bound microbubbles were imaged. This method allowed

Biomedical Optics EXPRESS

us to obtain clear bubble images with confocal microscopy since there was no residual DiI impeding the signal. Although the confocal image in Fig. 3 is clear, it required a higher objective and a fluorescent label to obtain a clean image of the bubbles. In the MPM image the residual DiI makes no difference because MPM is detecting **only** the liquid to gas interface of the bubble due to the THG signal as observed in the emission spectrum in Fig. (3c). Since the image acquired from MPM can be obtained **label-free**, it makes it a promising solution for lipid microbubble detection.

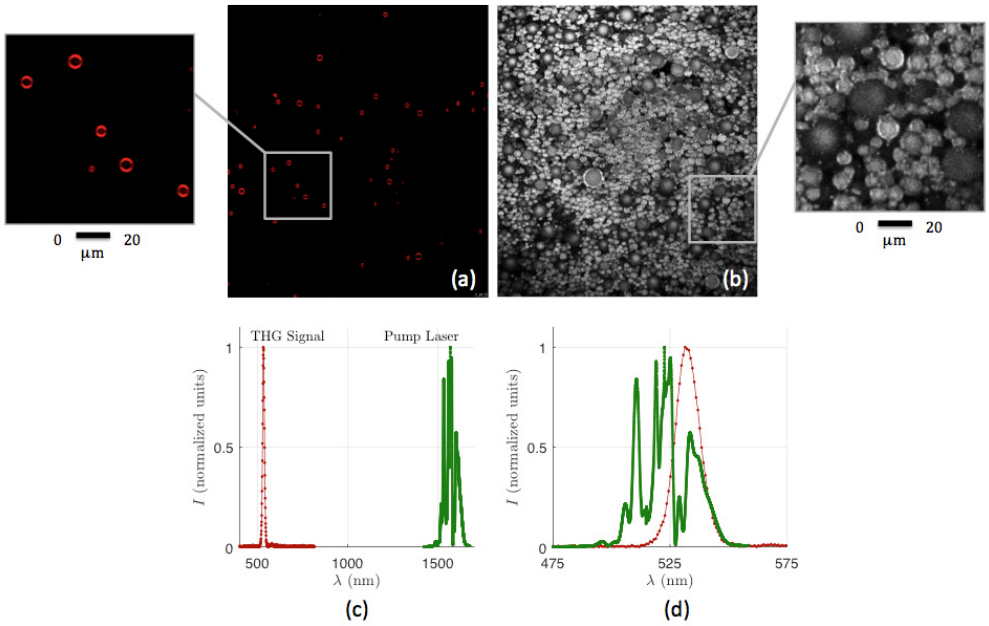

Fig. 3. Both upper images display lipid microbubbles conjugated with DiI. **(a)** Image taken by confocal microscopy where bubbles are dispersed and bound to a poly d-lysine cell culture plate with residual DiI washed away. **(b)** Image taken by multiphoton microscopy (using a 40x Nikon oil objective with a 1.3 NA), specifically THG, where many unbound microbubbles are floating in a solution. **(c)** Emission spectrum from 1560nm multiphoton microscope displaying emitted THG signal during microbubble imaging compared to the total pump laser. **(d)** The pump laser spectrum (divided by three) overlaid on the THG spectrum. In a perfect THG process, these curves would be identical. However, it is clear that the THG spectrum is cleaner than the pump laser, and this is likely due to chromatic dispersion, chromatic aberration, and the specific geometry of the focused field.

To verify that the signal obtained from MPM was specifically THG from the water/gas interface of the microbubbles, we performed another experiment with a lipid microbubble solution conjugated with DiI (a popular fluorescence marker) to prove colocalization between the fluorescent light channel and the THG channel. We used the 1040 nm laser to image the bubble solution with a 538 nm dichroic filter as well as a 345 nm bandpass THG filter. We chose the 1040nm laser over the 1560nm laser for this experiment because the 1040nm laser better excites the DiI signal. The beam split through the filters was such that the DiI signal appeared only in the fluorescent light channel and the THG signal appeared only in the third harmonic generation channel. Figure 4 shows the images obtained from this experiment as well as the emission spectrum. Figure 4(a) is an image of the THG channel, Fig. 4(b) is an image of the fluorescent light channel, and Fig. 4(c) is an image of a) and b) overlaid with THG represented in red and fluorescent light represented in green. Colocalization of the

Biomedical Optics EXPRESS

bubbles causes the bubble membrane to appear yellow. Figure 4(d) displays the emission spectrum, showing that the fluorescence signal we obtain is indeed from DiI.

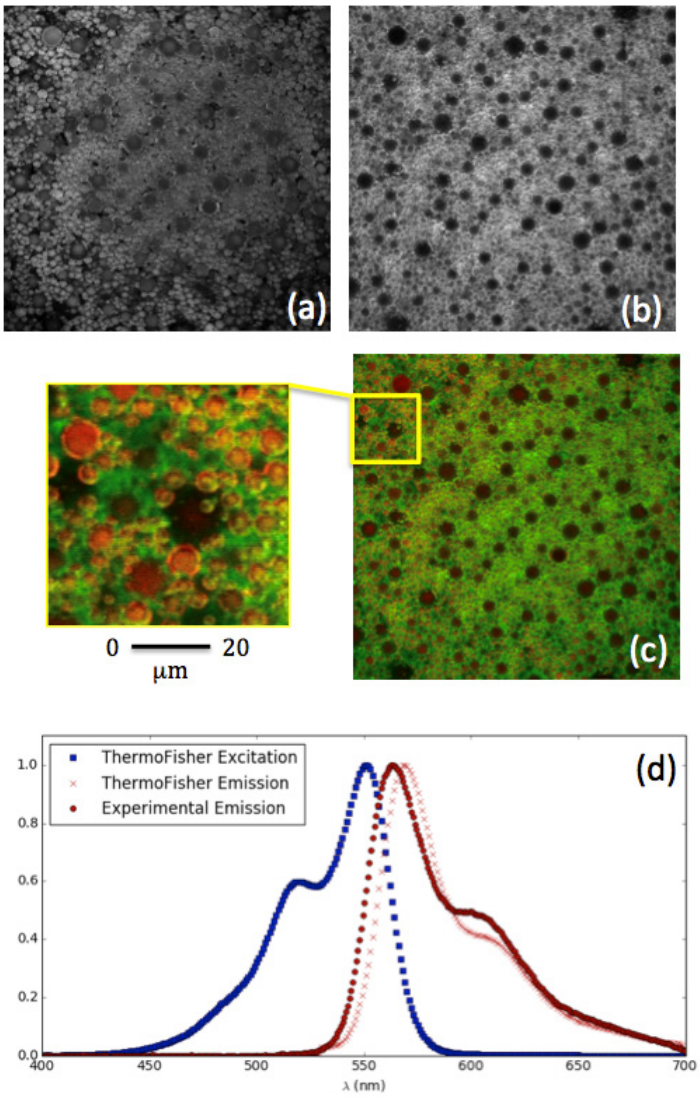

Fig. 4. Displays targeted lipid microbubbles conjugated with DiI. **(a)** The THG signal from the bubbles only **(b)** The fluorescence signal from the bubbles **(c)** A composite image of (a), represented in red, and (b), represented in green with the colocalized microbubbles represented with a yellow membrane **(d)** The measured emission spectrum of the DiI conjugated to the membrane of the lipid microbubbles compared to the thermofisher emission spectrum for DiI.

3.3 Confocal imaging of targeted and labeled lipid microbubbles to verify cell binding

To verify lipid microbubble binding to the cell strains, we first imaged with confocal microscopy. Twenty-four hours after the cells had been plated, the cells were rinsed with Dulbecco's phosphate buffered saline (DPBS) to remove debris from the microenvironment. Then the cells were incubated in DPBS for 30 minutes supplemented with 5 μl of calcein dye in addition to 100 μl of the lipid microbubbles conjugated with DiI. Due to the buoyancy of the microbubbles, the cells were inverted for this period to maximize exposure of the cells to

Biomedical Optics EXPRESS

the microbubbles. After the incubation period the cells were washed with DPBS to remove any unbound microbubbles and were then maintained in media for imaging.

The conjugation was finally visualized under the AZCC Leica SP5 confocal microscope (Leica Microsystems, Buffalo Grove, IL) with a 63x oil immersion objective captured at 2048x2048 pixels to obtain a field of view of 246.03x246.03 μm. The visible light wavelength lasers used were the 50 mW Argon laser (458, 477, 488, and 514 nm) and the 1mW Helium Neon Laser (543 nm) to capture the spectrum of the calcein (ex495/em515) fluorescing the cytoplasm of the living cells and DiI (ex549/em565) conjugated to the lipid microbubble membrane. Figure 5 displays the evident binding of the plectin-targeted lipid microbubbles to the pancreatic cancer cells.

3.4 Multiphoton imaging of bound microbubbles to verify the ability of THG to detect bubbles fixed on a cell surface

The technique of detecting lipid microbubbles using THG as a contrast mechanism was demonstrated by colocalization of the THG signal with the DiI fluorescence emitted from the microbubble membrane. In order to obtain separate DiI and THG signals, filters were placed in the multiphoton microscope to direct DiI fluorescence and THG into two PMT channels. These two channels were then combined in a false color image to show that the DiI signal and the THG signal from the membrane interface overlap thereby demonstrating dual and independent detection of label-free microbubble membranes.

The same procedure referenced elsewhere (Section 3.3) was used to prepare the cells for MPM imaging. The cells were visualized under the 1040 nm excitation multiphoton microscope with an oil immersion 40x objective (1.3 NA) with two filters to demonstrate THG generation can image plectin targeted lipid microbubbles. The filters used in the system were a 538 nm dichroic filter and the 345 nm bandpass THG filter. The 538 nm dichroic filter was used to send the fluorescent emission signals of the DiI on the bubbles and the calcein on the cells to one PMT detector. The THG filter was used to send the emission signal from the phase change of the bubbles to the other PMT detector. Figure 5 displays the images obtained from the two separate filters, a composite image of the filter combination, and an image from confocal imaging to compare to the final MPM image. Specifically, Fig. 5(a) represents the THG signal, Fig. 5(b) represents the fluorescent DiI signal, and Fig. 5(c) is the composite image of 5a (represented in red) and 5b (represented in green) so that the colocalized bubbles appear yellow. The presence of the yellow bubbles in Fig. 5(c) demonstrates colocalization and defines THG as a method of detection for lipid microbubbles.

Figure 5(d) is a comparison image taken with confocal microscopy of lipid microbubbles bound to pancreatic cancer cells. Although this image appears to be an equivalent or even superior imaging modality, the confocal image requires a fluorescent label and a higher NA of 1.4 (63x oil immersion) to obtain such a high resolution image. Multiphoton microscopy provides an image where the lipid microbubbles are easily detected without the use of a label, and also a high resolution image in comparison to the objective lens (Nikon 40x oil immersion) being used. Additionally, confocal microscopy is limited to the superficial cell layers of tissue due to scattering, absorption, and phototoxicity, whereas the infrared wavelengths used in multiphoton microscopy allow long-term time-lapse imaging [25]. The last portion of Fig. 5, part e, displays the excitation and emission wavelengths provided by Thermofisher for both fluorescent dyes used in the experiment, DiI and Calcein dye.

Biomedical Optics EXPRESS

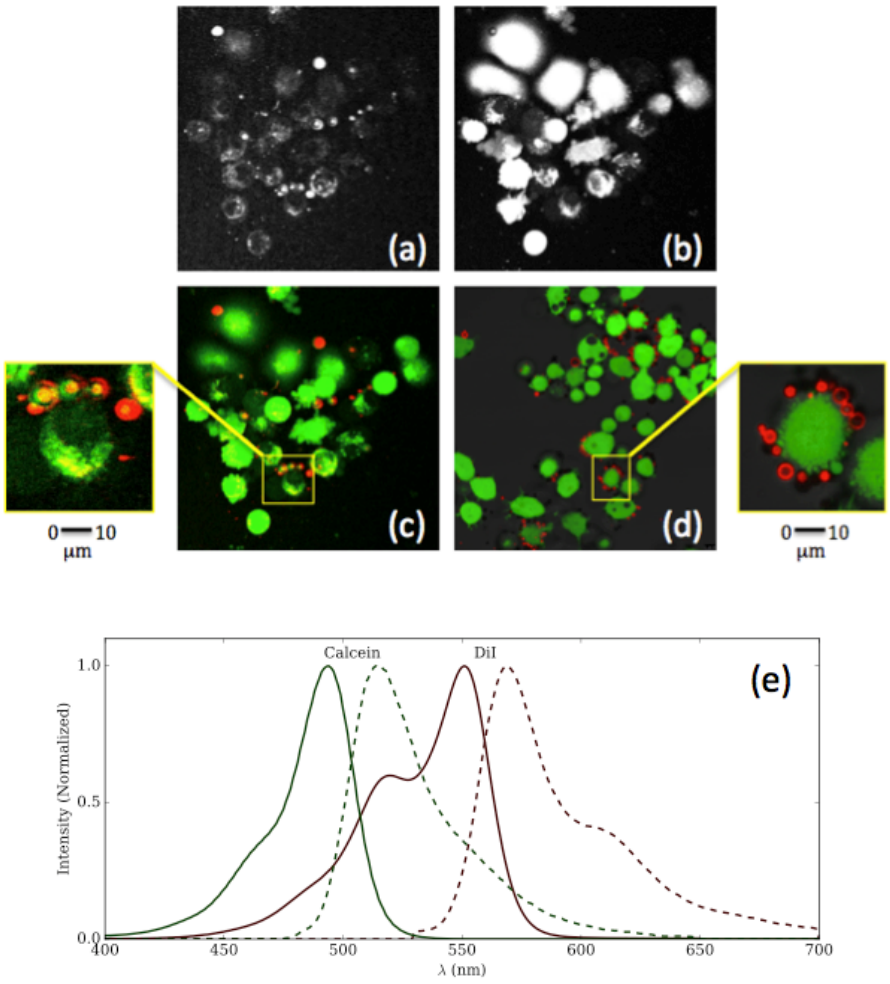

Fig. 5. Displays pancreatic cancer cells with the targeted lipid microbubbles bound to the surface of the cells. **(a)** The THG signal from the bubbles only **(b)** The fluorescence signal from the bubbles and cells **(c)** A composite image of (a), represented in red, and (b), represented in green with the colocalized microbubbles represented in yellow **(d)** An image obtained from confocal microscopy for comparison **(e)** A spectrum obtained from Thermo Fisher displaying the excitation and emission wavelengths of both calcein and DiI

4. Discussion

The contact-free detection of targeted lipid microbubbles was explored using the THG imaging modality of multiphoton microscopy. The results indicate that THG has the potential to generate images of microbubbles with a sensitivity equivalent to that of ultrasound. However THG offers superior spatial resolution relative to the same, therefore providing the potential to accurately detect one microbubble bound to a remaining cancerous cell. The contact-free detection of microbubbles with targeted attachment to cancer cells via surface receptors will increase the simplicity of imaging in a sterile, surgical environment as well as maintain the accuracy of detection.

The conventional method to determine if all the cancer has been resected during pancreatic surgery is based on frozen section microscopy of a tiny fraction of the surgical margin, which is subject to large sampling errors, and where seemingly clean margins are

Biomedical Optics EXPRESS

subsequently found to have cancer a few days later, when it is too late to re-do the operation. Although our study only covers cell work, this label-free detection method can be translated to imaging tissue samples, including pancreatic tissue in the operating room. Moreover, the development of this device into a hand-held probe will provide the mobility required to integrate MPM into a surgical setting, making it a potential method for point-of-care diagnostics [26, 27]. Overall, this point-of-care diagnostics method will improve cancer-free survival in pancreatic cancer patients and reduce the cost of care [28].

5. Conclusion

We believe these are the first reported label-free images of microbubbles detected by THG. Our preliminary results indicate that contact-free THG images of microbubbles attached to tumor cells may enable unseen cancer to be detected during surgery. With the development of MPM into an endoscopic probe, we believe this novel application could be translated to a wide variety of uses in point-of-care diagnostics as well as early detection of cancer.

Acknowledgments

This was supported in part by a Seed Grant from the Department of Medical Imaging, the Harry Barrett fellowship, and the State of Arizona TRIF funding.